FINITE ELEMENT FRACTURE MECHANICS ANALYSIS OF CREEP RUPTURE OF FUEL ELEMENT CLADDING*

P.S. CHOPRA

Analysis Department, Experimental Breeder Reactor Project, Argonne National Laboratory, Argonne, Illinois 60439, U.S.A.

SUMMARY

A finite element fracture mechanics technique is applied for simulating the elevated temperature creep rupture behavior of initially defected austenitic stainless steel fuel element cladding. The basic analytical approach consists of determining total instantaneous strain energy release rates, G_T, and the corresponding values of the stress intensity factor, K_T, from sequential linear elastic finite element solutions and relating these to either an effective creep fracture toughness parameter G_{ec} (or K_{ec}) or to creep crack growth rates, da/dt, obtained from test results.

An initial application of this approach has been made to simulate the creep rupture behavior of initially defected type 316 austenitic stainless steel fuel element cladding in the 20% cold worked condition, tested at 650 °C. This application has provided a relationship in the simple familiar form:

$$\sigma = \frac{K_{ec}(a/h,\, t_r,\, q)}{\sqrt{\pi}\,\sqrt{a}\;\; F(a/h)}$$

where σ is the nominal loop stress, a is the initial depth of a longitudinal crack, h is the cladding thickness, t_r is the time to rupture, and q is a structure sensitive parameter which accounts for the influence of the environment. $F(a/h)$ is a function, obtained from finite element solutions, which accounts for the geometric differences between the present structure and the classical Griffith plate. The function K_{ec} $(a/h,\, t_r,\, q)$ is obtained from creep rupture tests of cladding with varying initial flaw depths and times to rupture, under corrosive as well as inert environments.

Performing time-dependent analyses, a preliminary relationship is obtained between the instantaneous values G_T and K_T, and crack growth rates under corrosive and non-corrosive environments.

The analytical predictions of critical combinations of cladding flaw configurations, stresses, times to rupture and crack growth rates are in good agreement with the limited test data available for comparison. Current applications are aimed at the long-term cyclic creep fracture behavior of fast reactor fuel elements, using a non-linear finite element code. In addition, multiple intergranular fracture configurations are being investigated.

* This work has been performed under the auspices of the U.S. Atomic Energy Commission.

1. Introduction

The presence of grain boundary attack or material defects in fuel element cladding is of concern to designers and operators of nuclear reactors, since these material discontinuities can result in the premature termination of the service life of the fuel element. Until the technology can be developed to eliminate grain boundary attack and material defects, their influence on the lifetime performance of the fuel element must be accounted for in assuring its safe life. A conventional approach to this problem has been to reduce the effective clad thickness by an amount equal to the expected depth of the attack or material defect and compute the corresponding higher nominal stress, which is compared with the allowable stress. This approach can lead to unconservative estimates of the cladding's ability to withstand creep fracture as is demonstrated by the results presented in this study.

An alternate approach for evaluating the creep fracture performance of defected fuel element cladding is provided by the use of finite element fracture mechanics techniques which are capable of considering directly the influence of material defects and cracks and their propagation.

The present study evaluates the structural integrity of defected fuel element cladding experiencing creep at elevated temperatures with an objective of developing an analytical model relating defect size and location, nominal hoop stress or internal pressure, and time to rupture. The analytical tools employed are the finite element method of stress analysis and linear elastic fracture mechanics. In addition, the definition of an effective cladding creep fracture toughness is introduced to account for crack tip yielding and creep deformation.

2. Analysis Approach

Total instantaneous strain energy release rates for a structure experiencing fracture can be computed from a generalization of Griffith's energy criterion, coupled with finite element solutions of the strain energy stored in the structure for incremental fracture propagation configurations [1,2,3]. The generalized fracture criterion can be expressed in terms of the Hartz function, H_T:

$$H_T = G_T - R_T \geq 0 \tag{1}$$

where G_T is the total instantaneous strain energy release rate, and R_T is the rate at which energy is required for the formation of new fracture surfaces.

Strain energy release rates are evaluated by direct calculation of total strain energies, U_T, associated with finite element solutions of sequential boundary value problems using the relationship:

$$G_T = (\pm)* \frac{\Delta U_T}{\Delta a_T} \quad (2)$$

where Δa_T represents the total increment in the fracture surface area, a_T, including primary and secondary cracks. The method of computing U_T should account for all cracks as well as flaws present in the material. Since G_T is obtained by numerical integration in the internal Δa_T, the accuracy of the results depends upon the length of this interval.

The rate at which energy is required for crack formation, R_T, is a material property which depends upon the fracture path. Thus, R_T may be different for intergranular or transgranular fracture in corroded or uncorroded metals, or for fracture in non-homogeneous materials such as concrete or ceramics. An expression for R_T has been proposed in the form [1,2]:

$$R_T = \frac{[T_p\ (a_p)\ \Delta a_p + \sum_{j=1}^{m} T_{sj}\ (a_{sj})\ \Delta a_{sj}]}{\Delta a_T} \quad (3)$$

where $T_p(a_p)$ is the instantaneous specific surface energy of the primary crack, $T_{sj}\ (a_{sj})$ is the instantaneous specific surface energy of the jth secondary crack, and Δa_p and Δa_{sj} are the increments in the primary and secondary crack surface areas, a_p and a_s, respectively.

For most service applications, the value of R_T as defined by equation (3) cannot be easily determined. This is due to the uncertainty associated with the material's response to fracture under service conditions. Examples of these uncertainties are stress-corrosion, metallurgical changes resulting from exposure to elevated temperatures and/or irradiation, and local crack tip deformations, resulting from elevated temperature and/or irradiation induced creep and from plastic flow. Engineering approximations for the function R_T for a given service application, however, may be obtained from prototypical tests, using equation (1) with computed values of strain energy release rates G_T. In the current study, the engineering values of R_T, are obtained for type 316 stainless steel in the 20% cold worked condition, from creep rupture tests of initally flawed pressurized fuel element cladding.

The technique described, extends to multiple fracture configurations in nonhomogeneous and anisotropic materials. However, the current application is limited to longitudinal primary cracks originating from either the inner or the outer surface of austenitic stainless steel fuel element cladding.

3. Finite Element Simulation of Flawed Tubing

Total strain energy release rates were computed for pressurized 316 stainless steel tubing having an outer diameter of 0.25 in. and thickness of 0.015 in.,

* + for constant stress boundary conditions
  − for fixed displacement boundary conditions

containing longitudinal flaws of varying depths on the inner as well as the outer surface. Since a planar finite element representation was employed, it was assumed that the flaws are long compared with the tube radius.

The finite element code derived by Wilson [4], using the constant strain triangular element [5] was employed. A slight modification was made to this code to compute, internally, the strain energy stored in each element and its summation over the entire body.

The total instantaneous strain energy release rate, G_T, was computed from the difference in total strain energies stored for adjacent fracture configurations. When comparing two adjacent fracture configurations, the qualitative differences between the total strain energies computed for the two configurations were not expected to vary significantly with the finite element representation. Thus the use of a constant strain element for computing total strain energy release rates by the present method would induce less errors in the results than are present in previous applications where stress intensity factors or strain energy release rates were obtained directly from element centroidal stresses or nodal point displacements.

In order to avoid differences in the computed stresses and the total strain energy, U_T, due to mesh changes, the basic finite element mesh as well as the element and nodal point numbering was left unchanged. Primary crack extension was simulated simply by altering the boundary conditions for the node immediately ahead of the crack tip.

The influence of flaw depth and location on the maximum elastic uniaxial stress in an element immediately ahead of the tip of the flaw is shown in Figure 1. A single curve is presented for longitudinal external flaws and two curves are given for the case of longitudinal internal flaws. The curves for internal flaws illustrate the difference between internal pressure applied by a fluid and that applied by a frictionless mandrel. Under fluid pressure loading, the surface of the flaw will be loaded directly by the fluid, whereas under a mechanical load the surface of the flaw will be unloaded. Consequently higher crack tip stresses will be obtained under fluid pressure as compared to an equivalent mechanical load as shown in Figure 1. Stresses for both these cases are higher than those corresponding to an external flaw. The difference between the stresses obtained for the fluid pressure loading and the mechanical loading is small for smaller flaw depths and increases gradually with flaw depth. These results indicate the relative severity of gas pressure loading on internally flawed tubing as compared with fictionless mechanical loading.

Total strain energy release rates, G_T, for the fuel element cladding are shown in Figure 2 for external longitudinal flaws and for internal longitudinal flaws loaded by fluid pressure as well as by a frictionless mechanical load. Using the established relationships between the strain energy release rate,

G_T, for single cracks, and the Mode I stress intensity factor, K [6]:

$$K = \sqrt{G_T E} \text{ for plane stress*} \quad (4)$$

$$K = \sqrt{\frac{G_T E}{1-\nu^2}} \text{ for plane strain*} \quad (5)$$

where E is the modulus of elasticity and ν is the Poison's ratio; stress intensity factors can be obtained for the three cases studied. These are shown in Figure 3. An alternate approach for obtaining stress intensity factors is to relate the element stresses or nodal point displacements obtained from a single finite element solution, to the corresponding expressions for these quantities obtained from the literature. It has been shown, however, that this alternate approach can result in ambiguity primarily due to the several choices available for selecting the element or node for which the stresses or displacements are to be matched as well as the particular stress or displacement component to be matched [7]. Furthermore, stress intensity factors cannot be obtained directly for multiple fracture configurations [1].

Use of the stress intensity factor, K, as opposed to the strain energy release rate, G_T, however, is more convenient for engineering applications since it can be expressed directly in terms of stress. Consequently the criterion for fracture can be expressed in terms of the difference between the stress intensity factor, K, and the critical value of the stress intensity factor, K_c, or fracture toughness. The fracture toughness, K_c, corresponds to the rate at which energy is required for the formation of new fracture surfaces, R_T, or the energy fracture toughness parameter, G_c.

For comparison with the classical Griffith-Irwin solution for an infinite plate with a central crack, under uniform tension σ, it is convenient to express the stress intensity factors obtained in the present analysis in the form:

$$K = \sigma \sqrt{\pi} \sqrt{a} \; F(a/h) \quad (6)$$

where σ is the nominal hoop stress in the cladding obtained from a thin tube approximation and F (a/h) may be defined as a normalized stress intensity factor which accounts for the difference between the classical solution and the present solutions for internally or externally flawed pressurized tubing. Specifically, F (a/h) accounts for the presence of a non-uniform tangential and radial stress and for the tube curvature. The normalized stress intensity factors for the three cases studied are shown in Figure 4.

*Thus stress intensity factors for plane stress and plane strain vary only by a constant.

4. Application to Creep Fracture

The Griffith criterion of rupture states that fracture will occur when the strain energy release rate reaches a critical threshold, G_c, which, for perfectly brittle fracture, is the specific surface energy of the material [8]. Equivalent to the Griffith criterion for rupture is the premise that fracture will occur when the stress intensity factor defined by equation (6) reaches a critical fracture toughness threshold, K_c. In order to apply this fracture criterion to an engineering structure or component, it is necessary to characterize the fracture toughness for the range of loading conditions and environments expected during service, with the help of service experience or prototypical tests. A criterion for the creep fracture of flawed tubing under internal pressure may be expressed as:

$$\sigma \sqrt{\pi} \sqrt{a} \; F(a/h) \geq K_c \; (a/h, \; T, \; t_r, \; Q) \qquad (7)$$

where a/h represents a dependence on the structural configuration, T represents the temperature dependence, t_r, the time to rupture, represents a loading dependence related to the applied stress and strain rate, and Q represents the corrosive activity of the surrounding media. For applications at constant temperature and under a constant environment the expression (7) reduces to the form:

$$\sigma \sqrt{\pi} \sqrt{a} \; F(a/h) \geq K_{ec} \; (a/h, \; t_r) \qquad (8)$$

where K_{ec} is the "effective" creep fracture toughness for the specimens under consideration. It can be argued correctly that if K_{ec} is a material property, it should not be dependent upon the structural or fracture configuration and that any such dependency derives from the approximate expression, shown in the left-hand side of the inequality (8), for the <u>true</u> stress intensity factor. However, within the limits of currently available analytical techniques it appears unlikely that the dependence of K_{ec} on the fracture configuration can be eliminated entirely in the present application. This is due in part to the work expended in plastic and creep deformations which cannot be accounted for in a linear elastic finite element solution, and to the influence of observed multiple secondary fractures ahead of the primary propagating flaw [9]. In general, the stress intensity factor and the corresponding value of the fracture toughness are a function of the fracture configuration [1,2,3].

A practical engineering solution is obtained by postulating that the simplifying approximations of a linear elastic planar stress analysis for a single primary initial flaw can be accounted for indirectly by the effective engineering fracture toughness value K_{ec}, for the cladding, which can be determined from creep rupture tests and characterized as a function of flaw configuration a/h, and time to rupture, t_r. Based upon this hypothesis, a semi-emperical criterion for the creep rupture of initially flawed fuel element cladding can be expressed in the simple form:

$$\sigma \geq \frac{K_{ec}\ (a/h,\ t_r)}{\sqrt{\pi}\ \sqrt{a}\quad F(a/h)} \tag{9}$$

or

$$p \geq \frac{h}{r}\ \frac{K_{ec}\ (a/h,\ t_r)}{\sqrt{\pi}\ \sqrt{a}\quad F(a/h)} \tag{10}$$

where p is the internal pressure and r is the inner radius of the cladding.

5. Determination of Effective Cladding Creep Fracture Toughness

The expressions (9) or (10) can be used readily to determine the effective cladding fracture toughness from creep rupture tests of pre-cracked or pre-flawed tubing. In the present studies, the creep fracture results reported by King et al. [9] for 316 stainless steel tubing were used to determine K_{ec} values for various flaw depths and rupture times. Since these tests were limited in number and did not provide continuous data for varying crack depths, hoop stresses and rupture times, it was necessary to interpolate. The effective cladding fracture toughness K_{ec} (a/h, t_r) was determined in the form of the family of curves of K_{ec} vs a/h for various rupture times, shown in Figure 5, using the results of the internally flawed tubes reported by King et al. The effective fracture toughness values shown in Figure 5 are higher for shorter rupture times. The curves have a characteristic hump implying that K_{ec} initially increases with crack depth up to a maximum and then decreases. This maximum value of K_{ec} occurs at shorter crack lengths as the rupture time increases. In addition, the absolute values of these maxima's decrease with increasing rupture times.

An explanation for the behavior of the function K_{ec} (a/h, t_r) can be obtained by recognizing the limitations of the present elastic stress analysis and by considering the macroscopic fracture behavior of the defected cladding. At a constant time to rupture the initial increase in K_{ec} with flaw depth may be due to the increasing plastic zone at the crack tip and creep deformation. As the flaw depth is increased further, the effective fracture toughness may decrease due to the occurrence of multiple secondary cracks ahead of the primary flaw as observed in the present tests by King et al. [9] or due to the possible growth of voids as discussed by McClintock and Irwin [10]. This will result in an intensification of the stress and strain fields ahead of the primary flaw [1] and since the present solution considers only the primary flaw, the influence of these secondary cracks will appear as a decrease in the effective fracture toughness.

For constant flaw depth, the fracture toughness decreases with increasing rupture times. This may be due to the decrease in the nominal stresses to rupture at longer times, resulting in decreased crack tip yielding. This suggests further that at considerably longer rupture times the effective creep fracture toughness eventually may approach a threshold similar to the brittle fracture toughness of the material.

6. Results

6.1 Application of Effective Creep Fracture Toughness

The effective cladding creep fracture toughness curves shown in Figure 5 were used in conjunction with equation (9) or (10) to predict the creep fracture stress for type 316 stainless steel cladding in the 20% cold worked condition. The test results utilized included internal and external longitudinal electro-discharge machined flaws ranging in depth from approximately 10% to 50% of the wall thickness [9]. All the tests were conducted at 650°C in a He-1% O_2 atmosphere and internal pressurization was accomplished with either helium or argon.

A comparison between the predicted and the demonstrated hoop stress to cause rupture at specified times to rupture is shown in Figure 6. The solid circles correspond to internally flawed specimens and show good agreement between analytically predicted values and test data. This is to be expected since the effective cladding fracture toughness, K_{ec}, defined in equations (9) and (10), was obtained from the same set of specimens with internal flaws. However, application of the same effective fracture toughness curves to externally flawed specimens results in predicting stresses to rupture consistently higher than demonstrated values as is shown by the open triangles in Figure 6. This apparent discrepancy between predicted and demonstrated rupture stresses for externally flawed specimens may be explained by examining the normalized stress intensity factor, F (a/h), and the effective cladding creep fracture toughness, K_{ec}, in equations (9) and (10).

The normalized elastic stress intensity factor for an external longitudinal flaw is lower than that corresponding to a similar internal flaw. This is a consequence of the stress and strain distributions in the pressurized cladding and is reflected in the strain energy release rates discussed earlier. Thus for the same value of effective fracture toughness for an internal or an external flaw, based upon an elastic analysis, cladding with an external flaw is expected to withstand a higher stress to rupture than that with a similar internal flaw for the same time to rupture. This is accounted for in equation (9) by the use of the appropriate value of F (a/h), obtained from finite element solutions, shown in Figure 4.

In the tests conducted by King et al. [9] the cladding specimens with external flaws ruptured at lower stress levels than those corresponding to specimens with internal flaws of the same depth and for similar rupture times.

This may be explained by the experimenter's observation of the formation of an oxide film on the outer surface of the specimens resulting from reaction with the He - 1% O_2 environment. It should be noted that the environment on the inner surface of the specimens was relatively inert due to the use of either helium or argon as a pressurizing agent. It may be surmised therefore that the relative reduction in the fracture stress for the externally flawed specimens resulted from the activity of the corrosive media on the outer surface of the cladding.

The difference between predicted and demonstrated fracture stresses for the externally flawed specimens may provide an estimate of the activity of the corrosive media measured as a reduction in the effective creep fracture toughness. This reduction may be expressed as the ratio of the effective creep fracture toughness values, shown in Figure 5 for internal flaws in an inert atmosphere, to the demonstrated values for external flaws in the corrosive environment. The ratio, which may be termed the corrosion reduction factor, C*, is shown in Figure 7 as a function of the stress to rupture. It is seen that for a flaw depth of approximately 10% of the clad thickness, C decreases with increasing stress to rupture. This may indicate a decreasing influence of the corrosive activity as the stress field is intensified. It should be noted also that the factor, C, diminishes with decreasing time to rupture. For flaw depths of approximately 34% of the clad thickness, the corrosion reduction factor appears to be insensitive to rupture stress and the time to rupture. It appears in addition, that the corrosion reduction factor, C, is higher for specimens with smaller initial flaw depths for the same stress to rupture. This again may be indicative of the relative increase in the role of corrosion under decreasing crack tip stress field intensities and increasing times to rupture.

The observations made in Figure 7 may be utilized to modify the predictions shown earlier, for externally flawed specimens, to account for the suspected activity of the corrosive media. The effective fracture toughness values obtained for internal flaws therefore were modified by the use of the corrosion reduction factor, C, shown in Figure 7. The resulting predictions for the fracture stress are shown by the solid triangles in Figure 6.

6.2 Creep Facture Kinetics

In addition to consideration of the initial fracture and structural configuration of the fuel element cladding, the influence of time-dependent changes in the fracture configuration, the stress and strain fields and the strain energy release rate or the stress intensity factor, also must be considered. The strain energy release rates and the corresponding stress

*It should be noted that this factor may change if a non-linear analysis is employed.

intensity factors will be modified as a result of strain redistribution due to creep. This modification is expected to lower the strain energy release rate. Simultaneously, the strain energy release rate is expected to increase with crack growth, which again is a kinetic process. A sophisticated analysis of creep-fracture therefore must account for both these competing kinetic mechanisms which determine the instantaneous value of the total strain energy release rate as a function of the creep fracture process.

During creep controlled crack growth, the resistance of the cladding to fracture propagation may be expressed as the rate at which new fracture surfaces are formed, da/dt. These crack growth rates then can be related to the instantaneous value of the strain energy release rate, or the stress intensity factor, to characterize the fracture process.

An initial attempt has been made to develop the K - da/dt relationship for the creep rupture of defected fuel element cladding using the tests described in reference [9] and the stress intensity factor solutions presented earlier. Crack growth rates have been inferred from tests on different specimens tested at the same stress levels with varying initial crack depths. Thus it has been assumed that the crack growth kinetics for a specimen with an initial flaw depth of a_2 mils are the same as those for a specimen with an initial flaw $a(a_1 < a_2)$, after it has propagated to a depth of a_2 mils.

The inferred crack growth rates are divided into several time intervals. The rate of crack growth da/dt and the corresponding value of the stress intensity factor, K_{av}, for the crack configuration at the average of each time interval are computed. The resulting relationship between K_{av} and da/dt is shown in Figure 8, at different nominal hoop stresses for both internal and external flaws. It may be noted that the crack growth rates for the external flaws, due to the presence of a corrossive environment, are higher than those for the internal flaws. The accuracy of the results shown in Figure 8 will improve as the time intervals used for computing da/dt and K_{av} are reduced.

A more realistic evaluation of the creep fracture growth process and the K - da/dt relationship will be provided by considering the time-dependent changes in the strain energy release rates and the stress intensity factors as a consequence of the redistribution of the stress and strain fields due to the creep deformation process. The influences of these changes are currently being studied with the help of a finite element code developed by Sutherland for performing creep analysis of planar and axisymmetric structures [12].

7. Discussion

The application of a finite element fracture mechanics technique to the creep rupture of fuel element cladding represents an initial effort towards obtaining engineering solutions to the creep rupture problem, for the use of designers. However, the general limitations of the current approach must be noted. Some of these limitations and their influence on the applicability of the approach presented are discussed below.

In applying a fracture mechanics approach to the study of fracture in any structure, an initial flaw or crack must be assumed to be present in the structure. In fast reactor fuel elements, intergrannular attack has been observed to develop on the inner surface of the cladding during its irradiation lifetime [11]. Whether or not this attack is as severe as an identical configuration of multiple secondary fractures, the possibility of having an initial clad flaw early in the lifetime of a fuel element must be accounted for. Since, due to the nature of the stress field, the primary cracks are expected to be longitudinal, this configuration was selected for the present study. Future studies will involve the analysis of more complex flaw configurations using two-dimensional as well as three dimensional finite element models [1,13].

The influence of advance secondary fractures on the computed strain energy release rates and stress intensity factors has not been considered in the present analysis. Since advance secondary fractures were observed in test results used in this study [9] their influence has been accounted for indirectly in the effective fracture toughness values. However, a direct evaluation of multiple fracture configurations can be made with the use of generalized finite element energy rate approach presented earlier [1,2,3]. This will be reflected in the appropriate expression for the normalized stress intensity factor, F (a/h), in equations (9) and (10).

The nature of the effective creep fracture toughness curves developed in the present application suggest why burst or short term tests on notches specimens often fail to identify the influence of defects. The use of an effective thickness equal to the thickness of the undefected portion of the tubing, results in predicted internal pressures to rupture which are consistently unconservative for the tests conducted by King et al. [9] at rupture time greater than 10 hours. This lack of conservatism increases with initial flaw depth and time to rupture.

The current semi-emperical finite element fracture mechanics model provides a consistent correlation between predicted and demonstrated rupture stresses over a wide range of initial flaw depths and times to rupture. In addition, some indication is provided about the influence of stress corrosion on the creep fracture behavior of defected cladding. It should be noted, however, that some of the trends observed on the basis of the current initial investigation cannot be confirmed without additional analyses and information from tests or service experience.

The preliminary investigation of creep fracture kinetics of the fuel element cladding suggests that the failure time is a function of the crack growth kinetics and the critical value of the total instantaneous strain energy release rate or the corresponding stress intensity factor for fracture instability.

8. Conclusions

The finite element fracture mechanics technique presented is an initial attempt at simulating the creep rupture behavior of defected fuel element cladding. A simple relationship has been obtained between the initial flaw configuration, the nominal hoop stress, and time to rupture. This relationship hinges upon the effective creep fracture toughness parameter, K_{ec}, obtainable from representative cladding creep rupture tests. However, once this parameter has been characterized, the technique permits the simulation of other specified initial flaw configurations through the use of normalized stress intensity factors, F (a/h), obtained from finite element solutions.

The present study indicates that non-linear finite element analyses which include the influence of secondary fractures will result in improved definitions of the stress intensity factors, F (a/h). This will require a recalibration of the effective creep fracture toughness parameter, K_{ec}. Creep fracture kinetics may be evaluated more realistically by a consideration of the time-dependent changes in the fracture and structural configuration, and the corresponding values of the stress intensity factor. Additional analytical and experimental work is required in this area.

The results predicted by the current model appear to be in good agreement with test results over the range of initial flaw depths and times to rupture available for comparison. Furthermore, the technique directly accounts for the initial flaw configurations and the times to rupture, which are not accounted for by conventional approaches based upon effective thickness reduction, or lifetime or stress modification factors.

Acknowledgments

The author wishes to acknowledge the enlightening discussions and useful suggestions provided by Dr. J. R. Honekamp of the Experimental Breeder Reactor Project at the Argonne National Laboratory. Discussions with Professor B. J. Hartz of the University of Washington also are appreciated.

References

[1] Chopra, P. S., Finite Element Simulation of Secondary Cracking During Brittle Fracture, Ph. D. Dissertation, University of Washington, Seattle, 1971

[2] Hartz, B. J. and Chopra, P. S., "An Analytical Technique for Parametric Investigation of Multiple Fracture," Proc. Int. Conf. Mech. Behav. Matls., Kyoto, Japan, August 1971, Vol. I, pp. 357-369.

[3] Hartz, B. J. and Chopra, P. S., "A Finite Element Contribution to Fracture," Proc. 2nd U.S.-Japan Sem. Matrix Methods of Strl. Anal. Berkeley, August 1972, in Advances in Computational Methods in Structural Mechanics and Design, J. T. Oden, R. W. Clough and Y. Yamamoto, Editors, University of Alabama in Huntsville Press, 1972, pp. 457-472.

[4] Wilson, E. L., "Structural Analysis of Axisymmetric Solids," AIAA Journal, Vol. 3, No. 12, December 1965.

[5] Turner, M. J., Clough, R. W., Martin, H. C., and Topp, L. J., "Stiffness and Deflection Analysis of Complex Structures," J. Aero, Sc., Vol. 23, No. 9, 1956.

[6] Paris, P. C. and Sih, G. C., "Stress Analysis of Cracks," in Fracture Toughness Testing and its Applications, ASTM STP No. 381, April, 1965, pp. 30-81.

[7] Vatwood, V. B., "The Finite Element Method for Prediction of Crack Behavior," BNWL-SA-2383, Battelle Memorial Institute, February, 1969.

[8] Griffith, A. A., "The Phenomena of Rupture and Flow in Solids," Phil. Trans. Roy. Soc., 1920, pp. 163-198.

[9] King, R. T., Cook, K. V., and Reimann, G. A., "Biaxial Creep-Rupture Properties of Defective Stainless Steel Tubing," ORNL-TM-3711, Oak Ridge National Laboratory, April 1972.

[10] McClintock, F. A., and Irwin, G. R., "Plasticity Aspects of Fracture Mechanics," in Fracture Toughness Testing and its Applications, ASTM STP No. 381, April 1965, pp. 84-113.

[11] Evans, E. A., Kitner, E. E., Zebroski, E. L., Neimark, L. A., and Cox, C. M., "The Status of Engineering Design and Irradiation Testing of the Stainless Clad Mixed-Oxide Fuel System for Fast Breeder Reactors," Proc. 4th Int. Conf. Peaceful Uses of Atomic Energy, Geneva, September 1971, 2.10-1.

[12] Sutherland, W. H., "A Finite Element Computer Code (Axicrp) for Creep Analysis," BNWL-1142, Battelle Memorial Institute, October 1969.

[13] Wilson, E. L., "Solid Sap - A Static Analysis Program for Three Dimensional Solid Structures," Report to Denver Mining Res. Center, September 1971.

C 2/

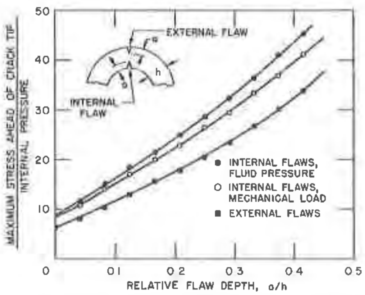

Fig. 1. Influence of Flaw Depth and Location of the Maximum Elastic Stress in the Cladding

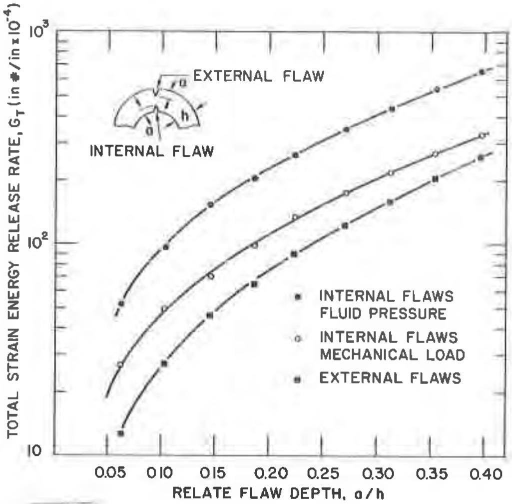

Fig. 2. Total Strain Energy Release Rates for the Propagation of Internal and External Flaws

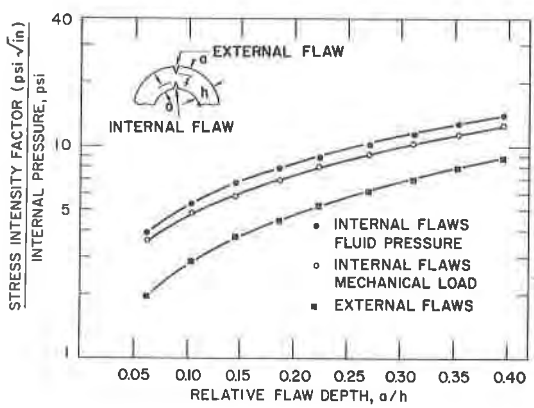

Fig. 3. Stress Intensity Factors for Internal and External Flaws

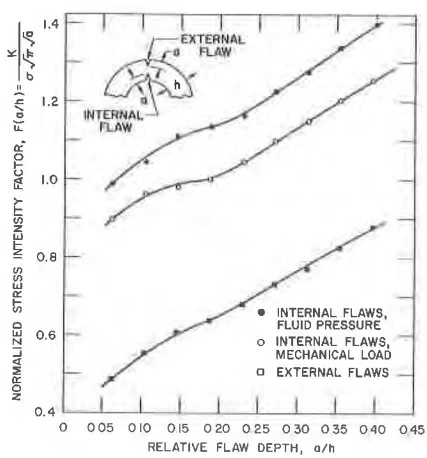

Fig. 4. Normalized Stress Intensity Factor for Internal and External Flaws

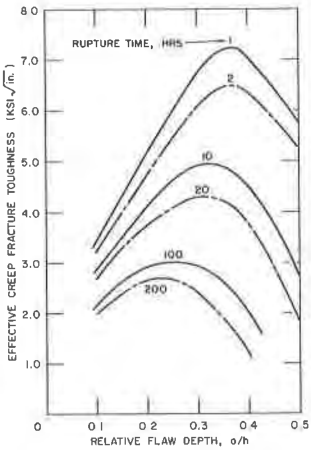

Fig. 5. Influence of Relative Flaw Depth and Time to Rupture on the Effective Creep Fracture Toughness

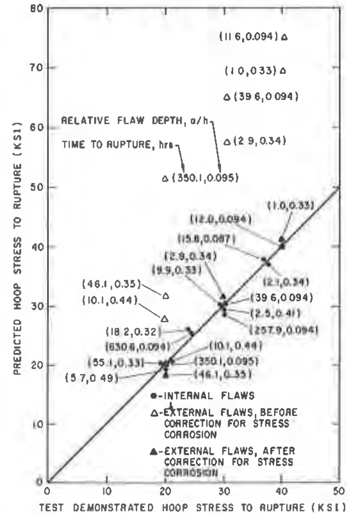

Fig. 6. Comparison of Analytical Predictions of Rupture Stress with Test Results

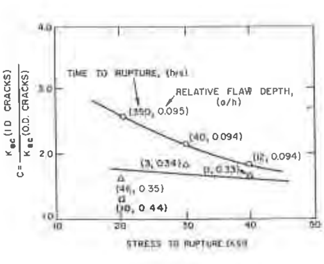

Fig. 7. Influence of Stress Corrosion on Effective Creep Fracture Toughness

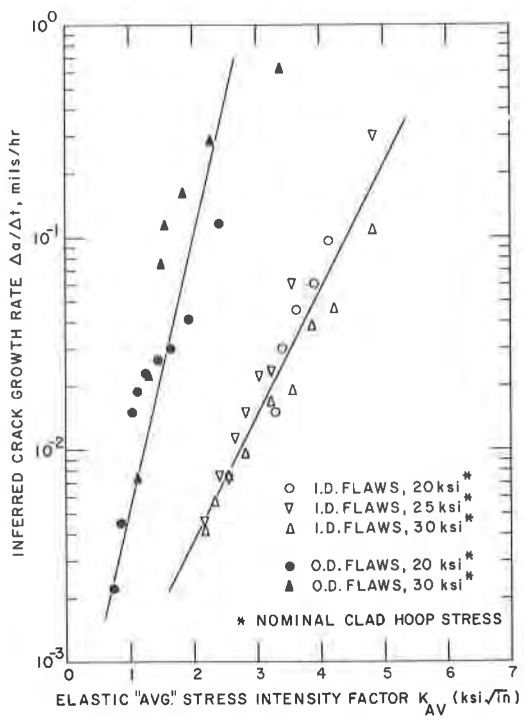

Figure 8: Inferred creep crack growth rates da/dt, at 650°C, in type 316 S.S. fuel element cladding as a function of the average elastic stress intensity factor, K_{av}.